

We are IntechOpen, the world's leading publisher of Open Access books Built by scientists, for scientists

6,900

Open access books available

186,000

International authors and editors

200M

Downloads

Our authors are among the

154

Countries delivered to

TOP 1%

most cited scientists

12.2%

Contributors from top 500 universities



WEB OF SCIENCE™

Selection of our books indexed in the Book Citation Index
in Web of Science™ Core Collection (BKCI)

Interested in publishing with us?
Contact book.department@intechopen.com

Numbers displayed above are based on latest data collected.
For more information visit www.intechopen.com



Physico - Chemical Modelling in Nonequilibrium Hypersonic Flow Around Blunt Bodies

Ghislain Tchuen¹ and Yves Burtschell²

¹*Institut Universitaire de Technologie F-V, LISIE, Université de Dschang, Bandjoun - Cameroun*

²*Ecole Polytechnique Universitaire de Marseille, Université de Provence, DME, 5 rue Enrico Fermi Technopole de Chateau Gombert, Marseille, France*
France

1. Introduction

The development of new space transportation vehicle requires better knowledge of hypersonic flow around blunt bodies and an accurate prediction of thermal protection system for extremely high temperatures. The complex domain of this hypersonic research program concerns the fully understanding and the control of reentry flowfield. The vehicle flying with high velocity through the upper layers of the atmosphere with low density. A very strong bow shock wave around vehicle is generated and converted the high kinetic energy into internal energy, thus increasing the temperature of the gas. Therefore, shock layer is the site of intensive physico-chemical nonequilibrium processes such as vibrational excitation, dissociation, electronic excitation, even the ionization and radiation phenomena. Under this typical hypersonic condition, air must be considered as a plasma around the vehicle which perturbs traditionally the communication between the vehicle and ground control station because the plasma absorbs radio waves. The computation of such flowfield is a challenging task.

The successful conception of such high technology would not have been possible without some knowledge of these thermochemical nonequilibrium phenomena and how they affect the performance of the vehicle. Some of these informations can either be obtained from experimental facilities such as wind tunnel and ballistic range, or large scale flight experiments, and/or numerical simulations. Moreover, small scale laboratory experiments are severely limited by impossible exact simulation of thermo-chemical nonequilibrium flow around a full scale hypersonic vehicle, and flight experiments are too costly to allow their widespread usage. Therefore, much of these aerothermodynamics informations needed to design future hypersonic vehicle will have to come from numerical predictions (the least expensive approach) which is a reasonable alternative after sufficient validations.

The numerical simulation of hypersonic flow in thermochemical nonequilibrium past a blunt body presents considerable difficulties for accurate solutions in the stagnation region. The computational results depend on the choice of the thermochemical model and the strategy of resolution. Generally, efforts provided to solve these types of flows have been based on the full coupling between Navier-Stokes equations and the thermochemical phenomena. Many

researchers have developed different thermal and chemical models for the description of hypersonic flowfield with the same experimental configurations. Therefore, it is important to determine an adequate model for accurate description of hypersonic flowfield.

Some of the largest uncertainties in the modeling of reacting hypersonic flow are the chemical reaction rates and the coupling between thermochemical phenomena. The uncertainties about the thermochemical processes render the calculations doubtful. Whereas methods for analyzing the aerodynamics in equilibrium flow have achieved a level of maturity, uncertainties remain in their nonequilibrium counterparts due to the incomplete modeling of chemical processes. Consequently, a good knowledge of the chemical modeling is required. For example, several chemical kinetics model give only the forward reaction rates. Many options are available for the calculation of the backward reaction rate with the equilibrium constant (Park[1], Gupta[2], Gibb[3]) and lead to different results. The method of computation of the backward reaction rate affects flowfield structure, shock shapes, and vehicle surface properties. It is necessary therefore, to make a judicious choice of an adequate model through a comparative study.

In the literature, a multitude of models for chemical kinetics of air exist. These models are built on different simplifying assumptions, and have all advantages and disadvantages depending on the problem simulated. The objective of the present study is to investigate results obtained with four different models of chemical kinetic. Solutions from models proposed by Gardiner[4], Moss[5], Dunn and Kang[6], and Park[7] are compared. Particular attention has been devoted to the way in which the backward reactions have been obtained. Gupta[2] high temperature least-squares equilibrium constant curves fits are also included. The influence of the formulations of Hansen[8], and Park[1] for the coupling between a molecule's vibrational state and its dissociation rate are compared. Several studies were presented in the past on the dissociation of nitrogen or of oxygen separately[9; 10]. The extension of these works to the complexity of overall reactions of air remains questionable. The present chapter attempt to identify the model with an acceptable confidence for a wide range of Mach number. The gas was chemically composed either by seven species ($O, N, NO, O_2, N_2, NO^+, e^-$) with 24 step chemical reactions or by 17 reactions involving five species (O, N, NO, O_2, N_2) and, or by nitrogen dissociated partially (N_2, N). One approach to validate the thermochemical model in CFD codes is to compare the shock standoff distance and the stagnation heating point along a sphere, with the experimental data.

Moreover, it has been shown that the description of the flow with a one temperature model leads to a substantial overestimation of the rate of equilibration when compared with the existing experimental data [1]. Much work on nonequilibrium flow are based on a model with two [11] or three [12] temperatures. For two temperature model, vibrational and electronic mode of molecules are described by a single temperature. This assumption is made to simplify the calculation. For the model at three temperature, it is assumed that a single temperature control the translational-rotational modes, a second temperature for vibrational mode for all molecules, and the third temperature for electronic-free electron modes. This was a reasonable assumption if the vibrational-vibrational coupling between the various molecular species is very strong. It is well known that the vibrational and electronic temperatures play important role in a high temperature gas because they improve the definition and evaluation of the physical properties of nonequilibrium hypersonic flow. In the present chapter, four-temperature model is used with two vibrational temperatures and the numerical results obtained for RAM C flight have well been compared with experimental data.

The results present in this chapter were obtained using an improved version of the time marching Navier-Stokes code CARBUR, originally developed at IUSTI Marseille. The code has been extensively tested in the past[13–16], and it's used here for the solutions of the stagnation-region flowfield. The scheme is based on a multiblock finite volume technique. The convective numerical flux is calculated by upwind technology with Riemann's solvers algorithms. The second-order central differences are used to discretize the viscous fluxes. An accurate second order algorithm in space and time is obtained by employing the MUSCL approach in conjunction with the Minmod limiter and the time predictor-corrector schemes. The source terms are treated implicitly to relax the stiffness. The steady state is obtained after convergence of the unsteady formulation of the discretized equations. We have included the recent definition and improvement in physical modelling. Special attention will be given to treatment of chemical phenomena that take place during reentry phase, in order to complete some description and modelisation of thermochemical nonequilibrium flow around atmospheric reentry vehicle.

2. Nomenclature

$A_{i,j}$	area of the cell (i, j)
A_r	constant for evaluating forward reaction rate coefficient $K_{f,r}$
$C_{v,q}^s$	specific heat at constant volume for species s for energy mode q , (where $q \equiv$ Translation, rotation, vibration, electronic)
$C_{p,q}^s$	specific heat at constant pressure for species s for energy mode q
D_s	diffusion coefficient of species s
$\rho e, e$	total energy per unit volume, mass
$\rho e_e, e_{e_s}$	electron-electronic energy per unit volume, mass of species s
$\rho e_{v_m}, e_{v_m}$	vibrational energy per unit volume, mass of molecules m
$H_{i,j}$	axisymmetric source term
$K_{eq,r}$	equilibrium constant for reaction r
$K_{f,r}, K_{b,r}$	forward and backward reaction-rate coefficient for reaction r
L_e	Lewis constant number, ($= \rho C_p D / \lambda$)
M_s	molecular weight of species s
NM	total number of molecules
N_k	outward normal vector on each side of the cell
NR	total number of reactions
NS	total number of species
NSV	total number of molecules in vibrational nonequilibrium
p_s	pressure of species s
Q_{T-e}	translation-electronic energy transfer rate
Q_{T-v_m}	translation-vibration energy transfer rate
Q_{v-v_m}	vibration-vibration energy transfer rate
$r_{i,j}$	radius of the cell-center position
T	Translational-rotational temperature
T_a	geometrically averaged temperature ($= T^q T_v^{1-q}$ or $= T^q T_e^{1-q}$)
T_e	electron-electronic excitation temperature
T_{v_m}	vibrational temperature of molecule m
t	time

U	vector of conserved quantities
u, v	velocity in x and y directions
Y_s	mass fraction of species s ($= \frac{\rho_i}{\rho}$)
<i>Greek symbols</i>	
λ_{tr}	translational thermal conductivity of mixture
$\lambda_{v,m}$	vibrational thermal conductivity of molecule m
λ_{el}	electronic thermal conductivity of mixture
ω_s	mass production rate for species s
$\alpha_{s,r}$	stoichiometric coefficient for reactant s in reaction r
$\beta_{s,r}$	stoichiometric coefficient for product s in reaction r
γ	ratio of specific heat ($\gamma = C_p/C_v$)
$\Omega_{i,j}$	source term
θ_r	characteristic temperature of reaction r
$\theta_{v,m}$	characteristic temperature of vibration
τ_m	average vibrational relaxation time of molecule m
$\tau_{m,s}^{VT}$	vibrational relaxation time for collision pair $m - s$
ρ	total density ($= \sum_s \rho_s$)
ρ_s	density of species s
<i>Subscripts</i>	
eq	equilibrium
m	molecule
s	species
w	wall
∞	freestream

3. Analysis

The governing equations that describe the weakly ionized, thermo-chemical nonequilibrium flow have been developed by Lee [17]. In this work, the following assumptions are introduced: 1) The flow regime is continuum. 2) The energy level of each mode are populated following boltzmann distribution with a characteristic temperature. 3) The rotational mode energy of molecules is fully equilibrated with the translational mode of heavy particles, and therefore translational and rotational temperatures of molecules are equal. 4) The harmonic oscillator model is employed for the vibrational energy. 5) The gas in the shock layer does not emit nor absorb radiation. 6) When ionization is taken into account, absence of the conduction current is assumed and an induced electric field is built up by charge separation [18], the magnitude of this field is predicted to be: $E_i \cong -\frac{1}{N_e e} \frac{\partial p_e}{\partial x_i}$.

The full laminar Navier-Stokes equations for two-dimensional conservation equations are written as:

The mass conservation equation for each species, s ,

$$\frac{\partial \rho_s}{\partial t} + \frac{\partial \rho_s u_j}{\partial x_j} + \frac{\partial \rho_s V_s^j}{\partial x_j} = \omega_s \quad (1)$$

The momentum conservation equation in x and y directions,

$$\frac{\partial \rho u_i}{\partial t} + \frac{\partial (\rho u_i u_j + p \delta_{ij})}{\partial x_j} + \frac{\partial \tau_{ij}}{\partial x_j} = \sum_s \epsilon N_s Z_s E_i \quad (2)$$

The total energy equation,

$$\frac{\partial \rho e}{\partial t} + \frac{\partial ((\rho e + p) u_j)}{\partial x_j} + \frac{\partial (u_i \tau_{ij} + q_{t_j} + q_{v_m j} + q_{e_j} + \sum_s^{ns} (\rho_s h_s V_s^j))}{\partial x_j} = \sum_s \epsilon N_s Z_s E_i u_i \quad (3)$$

The conservation equation of vibrational energy for each nonequilibrium molecule,

$$\frac{\partial \rho e_{v_m}}{\partial t} + \frac{\partial (\rho e_{v_m} u_j)}{\partial x_j} + \frac{\partial (q_{v_j} + \rho_m e_{v_m} V_m^j)}{\partial x_j} = Q_{T-v_m} + Q_{v_m-v_r} + Q_{v_m-e} \quad (4)$$

When the electronic relaxation is accounted, the electron-electronic energy conservation equation

$$\frac{\partial \rho e_e}{\partial t} + \frac{\partial ((\rho e_e + p_e) u_j)}{\partial x_j} + \frac{\partial (q_{e_j} + \sum_s \rho_s e_{e_s} V_s^j)}{\partial x_j} = u_j \frac{\partial p_e}{\partial x_j} - Q_{v_m-e} + Q_{T-e} + Q_{el} \quad (5)$$

In these equations, the electric field due to the presence of electrons in flow is expressed as:

$$\vec{E} \simeq -\frac{1}{N_e \epsilon} \vec{\nabla} p_e \quad (6)$$

The mixture is assumed to be electrically neutral ($\sum_s \epsilon N_s Z_s E_i \simeq 0$) as a consequence of the chemical kinetic mechanism; for each ion produced/consumed in the flow an electron is also produced/consumed. The local charge neutrality is also assumed. Thus, the number of electrons is equal to number of ions at each point:

$$\rho_e = \hat{M}_e \sum_{s=ions} \frac{\rho_s}{\hat{M}_s} \quad (7)$$

The state equation of the gas allows to close the system of equations (1-5). The total pressure is given as sum of partial pressures of each species regarded as perfect gas.

$$p = \sum_{s=1}^{NS} p_s = \sum_{s \neq e} \rho_s \mathcal{R}_s T + \rho_e \mathcal{R}_e T_e \quad (8)$$

The total energy of the mixture per unit volume

$$\rho e = \sum_{s \neq e} \rho_s C_{v,tr}^s T + \frac{1}{2} \sum_s \rho_s u_s^2 + \sum_{m=1}^{NM} \rho_m e_{v_m} + \rho e_e + \sum_{s=1}^{NS} \rho_s h_s^0 \quad (9)$$

is splitted between the translational-rotational, kinetic, vibrational, electron-electronic contributions, and the latent chemical energy of the species. T and T_e are deduced through the equation (5) and (9) with an iterative method. The vibrational temperature of the diatomic

species m is determined by inverting the expression for the energy contained in a harmonic oscillator at temperature T_{v_m} :

$$e_{v_m} = \frac{\mathcal{R}}{\hat{M}_m} \frac{\theta_{v,m}}{e^{\theta_{v,m}/T_{v_m}} - 1} \quad (10)$$

The speed of sound plays a major role in flux-split algorithm. It's evaluation in the case of one translational temperature is no longer applicable in the case of multiple translation temperature. The correction of the speed of sound due to electronic contribution and the presence of electron translational temperature has been included[19]:

$$a^2 = \gamma \left(\frac{p}{\rho} \right) + (\gamma - 1) \left(\frac{T}{T_e} - 1 \right) \frac{p_e}{\rho} \quad (11)$$

where classical speed of sound is obtained when $T = T_e$.

3.1 Transport coefficients

The transport coefficient modelling can have a considerable quantitative influence on practically relevant quantities such as skin friction and heat flux at the vehicle walls. Accurate measurements of transport coefficients at the high temperatures of interest for hypersonic applications are very difficult to realize and there is accordingly severe dearth of reliable experimental data for these thermophysical properties. Several useful simplifications have been used but their relevance and reliability, other than for quick estimates of order of magnitude, become rather questionable under increasingly advanced demands on accuracy. Some of the formulas in use become less reliable at high temperatures where ionization becomes important. In this study, the viscous stresses τ_{ij} are defined with the hypothesis of Stokes. The dynamic viscosity is given by Blottner[20] interpolation law. The thermal conductivity of each species is derived from Eucken's[3] relation. The Wilke's semi-empirical mixing rule[21] is used to calculate total viscosity and conductivity of the gas. For simplicity, the mass diffusion fluxes for neutral species are given by Fick's law with a single diffusion coefficient [19]. The diffusion of ions is modeled with ambipolar diffusion coefficient $D_{ion}^{ambi} = 2D_s$. To improve this formula, we used $D_{ion}^{ambi} = D_{ion}(1 + T_e/T)$ as recommended in[22]. The effective diffusion coefficient of the electrons (D_e) is proportional to the ambipolar diffusion coefficient of the ions [19].

The total heat flux is assumed to be given by the Fourier's law as:

$$\vec{Q} = \sum_s q_s = - \sum_s (\lambda_{tr,s} \nabla T + \lambda_{v,s} \nabla T_{v,s} + \lambda_{el,s} \nabla T_e + \rho D_s h_s \nabla Y_s) \quad (12)$$

which is the resultant of the flux of conduction, vibration, electronics and the diffusion of the total energy. After using an extension form of Masson and Monchick assumptions[23], and the relation given by Athye[24] to connect thermal conductivity of vibration with the diffusion coefficient, a more convenient form of the total heat flux is obtained as:

$$\vec{Q} = - \frac{\lambda'_{tr}}{C'_{pf}} \left[\nabla h + (L'_e - 1) \left(\sum_{s=1}^{NS} h_s \nabla Y_s + \sum_{s=1}^{NSV} Y_s \nabla e_{v,s} + \nabla e_e \right) \right] \quad (13)$$

Where the Lewis number $L'_e = \frac{\rho D C'_{pf}}{\lambda'_{tr}}$ represents the ratio of the parts of the heat flux due to the energy transport by the diffusion gas mixture components and by heat conduction which depends on the translational temperature, and $\lambda'_{tr} = \lambda_{tr} + \sum_{I=eq} \lambda_{v,I}$ (I : molecules in equilibrium); and the similar expression for $C'_{pf} = C_{p,ir} + \sum_{I=eq} Y_I C_{v,vib,I}$.

3.2 Energy exchange model

The energy exchange between translation and vibrational mode Q_{T-v} is described according to Landau-Teller theory[1]

$$Q_{T-v_m} = \rho_m \frac{e_{v_m}(T) - e_{v_m}(T_{v_m})}{\tau_m} \quad (14)$$

and τ_m is the relaxation time expressed as in reference[19].

The vibrational energy transfer between the different molecules is modelled by Candler[25]:

$$Q_{v-v_m} = \sum_{s \neq m} P_{sm} Z_{sm} \frac{\hat{M}_s}{\mathcal{N}} [e_{vs}(T_{vsm}) - e_{vs}] \quad (15)$$

where T_{vsm} is the same vibrational temperature obtained after the collision of the two molecules, Z_{sm} is the $s - m$ collision number per unit volume which is determined from kinetic theory[3], P_{m-s} and P_{s-m} are the two probabilities originating from the work of Taylor et al.[26]. These probabilities have been presented recently in an exponential form by Park and Lee[7].

When electron-electronic energy is taken into account, the expression of the energy exchanged during electron-heavy particles collisions is derived from Lee[17]

$$Q_{T-e} = 3\mathcal{R}\rho_e(T - T_e) \sqrt{\frac{8\mathcal{R}T_e}{\pi M_e}} \sum_{r \neq e} \frac{\rho_r N}{\hat{M}_r^2} \sigma_{er} \quad (16)$$

where σ_{er} are the collision cross sections for interaction electron-other particle. The value is assumed to be constant and equal to $10^{-20} m^2$.

Q_{e-v_m} is the energy source term from vibration-electron coupling. It is assumed that only $N_2 - e$ coupling is strong[17], and its expression is assumed to be of the Landau-Teller form :

$$Q_{e-v_m} = \rho_m \frac{\hat{M}_m}{\hat{M}_e} \frac{e_{v_m}(T_e) - e_{v_m}(T_{v_m})}{\tau_{em}}; \quad m = N_2 \quad (17)$$

where the relaxation time τ_{em} is a function of electron-electronic temperature and electron pressure as presented in[25]. The term Q_{el} accounts for the rate of electron energy loss when a free electron strikes a neutral particle and ionizes it, with a loss in electron translational energy.

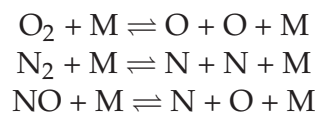
3.3 Chemical processes

The accurate characterization of the shock layer in hypersonic flow requires the good knowledge of the species mass, produced by chemical reactions which take place according to a suitable chemical kinetic model. An instantaneous accurate prediction of the mass fraction and the heating rate require a correct simulation of the chemical behavior of the flow field. The

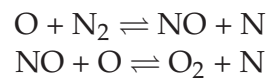
mechanism by which the considered chemical reactions appear is little known. Several ways lead to intermediate products or highly unstable excited states, which are available virtually for each reaction. It is difficult to produce theoretical formulations that involve all species, and to conduct experimental work for the kinetic data that shows the evolution of chemical reactions. Solutions from Dunn and Kang[6], the Gardiner[4], Moss[5] and Park[7] reaction rate sets are compared. All these models are different essentially in the data of the forward and backward coefficients of reactions rate. In Dunn and Kang, the ratio of rate is not necessarily equal to the equilibrium constant as required by Eq.19. A modified Dunn and Kang model, was created when the backward rate is computed either with exact or curve fit equilibrium constants. Three different models of chemical reactions are simulated in this study.

- The first model applied to 5 species (O, N, NO, O_2, N_2) with 17 elementary reactions are grouped into 15 reactions of dissociation and 2 exchange reactions.

- Dissociation

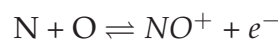


- Exchange or Zel'dovich reaction



M represents the collision partner which is one of the 5 species of the mixture.

- The second model is applied to 7 air species ($O, N, NO, O_2, N_2, NO^+, e^-$) with 24 elementary reactions. In this case, the reaction of ionization is added to the model above



- The last model is applied to the dissociation of nitrogen gas (N_2, N).

The increase or decrease of the species concentration due to chemical reactions is given by source terms ω_s as follows:

$$\omega_s = \hat{M}_s \sum_{r=1}^{NR} (\beta_{s,r} - \alpha_{s,r}) \cdot \left[K_{f,r} \prod_{s=1}^{NS} (\rho_s / \hat{M}_s)^{\alpha_{s,r}} - K_{b,r} \prod_{s=1}^{NS} (\rho_i / \hat{M}_s)^{\beta_{s,r}} \right]$$

where the associated forward and reverse reaction rate coefficients are assumed to satisfy the generalized Arrhenius law:

$$K_{f,r} = A_r T^{\eta_r} e^{-\theta_r/T} \quad (18)$$

Backward rates $K_{b,r}$ are defined either with curve fit constants in the Arrhenius expression, or with the equilibrium constant $K_{eq,r}$:

$$K_{eq,r} = \frac{K_{f,r}}{K_{b,r}} = \frac{\prod_{i=1}^{NS} (\rho_i / \hat{M}_i)^{\alpha_{i,r}}}{\prod_{i=1}^{NS} (\rho_i / \hat{M}_i)^{\beta_{i,r}}} \quad (19)$$

$K_{eq,r}$ can be determined analytically with the minimization of Gibbs free energy of each species under thermodynamics assumptions [3]. Moreover, for thermo-chemical nonequilibrium,

the theoretical formulation becomes poorly defined due to the complexity of the physical phenomenon. However, the fitting of experimental data would be more reliable than the theoretical formulation, because every simplification introduced in the thermodynamics model affects results.

According to Park, the equilibrium constant $K_{eq,r}$ is given by the following exponential polynomial

$$K_{eq,r} = \exp(A_{1,r} + A_{2,r}z + A_{3,r}z^2 + A_{4,r}z^3 + A_{5,r}z^4), \quad (20)$$

$$z = 10000/T$$

This Park curve fits were performed from data points only at 2 000, 4 000, 6 000, 8 000 and 10 000K. Gupta[2] has examined the curve fits for equilibrium constants to temperatures above 30 000K. He demonstrates that the five parameters used in both the Park reaction rate set and those derived from the Dunn and Kang[2] rates are incorrect at temperatures above 10 000K. Gupta least squares curve fitted, with a six parameters function for equilibrium constant is of the form

$$K_{eq,r} = \exp(a_{1,r}z^5 + a_{2,r}z^4 + a_{3,r}z^3 + a_{4,r}z^2 + a_{5,r}z + a_{6,r}) \quad (21)$$

The forward reactions rate of the dissociation of the nitrogen molecule are represented in Fig.1 and it is observed that the Dunn and Kang kinetic is largely separated from the others. The causes of uncertainties on the determination of the reactions rate coefficients are multiple, and is still rather poorly known. The present work examines various options for calculating the backward rates for several chemical kinetic models. The vibration - dissociation coupling is also considered in this chapter.

3.4 Vibration-dissociation coupling

The vibration - dissociation coupling is very important behind a strong shock in thermo-chemical nonequilibrium flow. Directly behind the shock, the translational temperature reaches a maximum value while the vibrational temperature takes a time to be excited before reaching its equilibrium value. Therefore, a model of dissociation depending only on the translational temperature will tend to overestimate total dissociation. The most important and poorly understood issue is how to model the coupling between a molecule's vibrational state and its dissociation rate. Many analyses of this coupling have been made in the past, either with more or less realistic and sophisticated physico-chemical models, or with semi-empirical methods easily usable in hypersonic computation codes[1]. There are perhaps 10 such models available in literature, however only the Park and Hansen models are used in this study.

Chemical reaction rates are affected by the extent to which the internal modes of atoms and molecules are excited. The coupling factor translating the influence of the vibration on dissociation is given by the ratio:

$$Z(T, T_v) = \frac{K_f(T, T_v)}{K_f(T)} \quad (22)$$

There are several methods for including thermal non-equilibrium effects in the chemical kinetic of air. Some have a semi-empirical origin, based on experimental results and

are often extrapolated well beyond their validity domains (without physical justification). Whereas those with analytical origin, arise from particle collision theory. Park[7] suggested a geometrically average rate controlling temperature T_a for dissociation reactions. T_a is defined as :

$$T_a = T^q T_{v_m}^{1-q} \quad \text{and} \quad K_{f,r}(T, T_{v_m}) = A_r T_a^{\eta_r} e^{-\theta_r/T_a} \quad (23)$$

with $q = 0.5$ in the original formulation. Sharma et al.[27] suggested that the value of q varied from 0.6 to 0.7 might be more realistic for high enthalpy flow and consequently, a value of 0.7 is used in the present study. Sharma's modification of the model is based on the analysis of experimental data for the reaction velocity observed in shock tubes. Hassen used collisional cross section theory to compute dissociation reaction rates up to 40,000K for flow in thermal nonequilibrium. He suggested an alternative formulation for the rate controlling temperature, similar to the Park approach

$$q = \alpha - \beta \left(\frac{T_v}{T} \right) \quad (24)$$

with α and β values reported in table 1.

The various values of the coupling factor for O_2 and N_2 at $T=20,000K$ are represented in Fig.2. Losev's[28] coupling is also included. As evident in Fig. 2, below 15,000K the magnitude of the coupling is very sensitive to the coupling model used.

4. Numerical methods

4.1 Numerical procedure

The governing equations (1-5) are discretized in space by using a finite-volume approach with a central formulation over structured mesh. The inviscid fluxes at cell interfaces are computed using AUFS[13] method. The second-order spatial accuracy is obtained by employing the monotonic upstream schemes for conservation laws (MUSCL-Hancock)[29] with a TVD extension type scheme approach. The limiter function Mimmod is used for the inviscid fluxes. The viscous terms are classically discretized by second-order central difference approximation.

The explicit formulation which gives the variation of $U_{i,j}$ during time Δt on each cell (i, j) can be written in two dimensional axisymmetric coordinate as:

$$\frac{\Delta U_{i,j}}{\Delta t} + \frac{1}{A_{i,j} r_{i,j}^\alpha} \sum_{k=1}^4 F_k N_k = \alpha H_{i,j} + \Omega_{i,j} \quad (25)$$

where $\alpha = 1$ for an axisymmetry coordinate system, and $\alpha = 0$ for planar two-dimensions. The source terms Ω is treated implicitly to relax the stiffness. A time predictor-corrector algorithm is used to obtain second-order time accuracy.

The structure of this code is multi-blocks and uses parallel processing machine architecture for significant enhancement of efficiency in treating of complex flow configuration. A detailed description of this numerical method may be found in [19].

4.2 Boundary conditions

The freestream conditions is hypersonic. The outflow is supersonic and the zero gradient exit condition is appropriate. Along the stagnation line, the flowfield is symmetric. The wall temperature (T_w) is fixed and zero normal pressure gradient is imposed. The no-slip and

no-temperature jump conditions are used. At the wall, the flow is generally assumed to be in thermal equilibrium. Because of the shielding effect, we have assumed either $T = T_{v_s} = T_e$ when vibrational and electronic energy content is greater than the electron translational energy content or $\partial T_{v_s}/\partial n = \partial T_e/\partial n = 0$ otherwise. The wall is supposed to be chemically noncatalytic. The upstream flow conditions, the number of nodes and the minimum grid spacing in x and y directions considered in this study are reported on Table 2. The distribution of points in the x and y directions of the computational domain is stretched exponentially in the region where there are strong shock interactions, while being clustered more near the surface to ensure y^+ for the first grid point less than 1.2. The time step is computed locally in each cell from a given CFL number. In each case, the free-stream air/nitrogen gas is composed of 79 % N_2 and 21 % O_2 or 92.7 % N_2 and 7.3 % N .

4.3 Condition of numerical simulation

The computational results are validated with experimental observations reported by Lobb[30], Rose et al.[31] and Hornung[32] for the shock standoff distance and surface heat transfer distributions. Results of the current numerical simulations are validated with the shock tunnel data presented in Table 2.

The first case study involves Lobb's experiment[30] devoted to the measure of shock detachment at 5.28 km/s. The second computation is also validated with the shock tube measurements of stagnation point heat flux for blunt bodies at 5.74 km/s from the work of Rose et al.[31]. The RAM-CII flight is a program conducted by the NASA Langley Research Center to assess the effects of black-out during re-entry. Computations were performed for RAM-CII conditions at Mach 25.9 for comparison with available numerical simulations. The case $M_\infty = 23.9$ is also included. This case has a relatively high density conditions of the flow field which leads to a high chemical reactivity. For the last case that involved hypersonic nitrogen flow over cylinders, the focus was to reconstruct the interferogram experiments performed by Hornung[32]. The results have been found to compare favourably with experimental results obtained with a free-piston driven shock tube wind tunnel which was used to obtain interferograms of the flow of pure nitrogen over blunt-nosed bodies. At the end, an extension is made for study the influence of the choice of chemical model for a hypersonic flow around a double-wedge.

5. Results and discussions

5.1 flow past blunt bodies

A grid resolution study was performed in the former work[14] to determine the number of points required for different cases. The current numerical algorithm was used to achieve grid independent solutions and for a flow in thermochemical nonequilibrium. The same CFD code and mesh points are used to examine the influence of all the current chemical kinetic models selected on flowfield structures, shock shapes, and vehicle surface properties. The results obtained are presented and compared with experimental data and numerical results.

5.1.1 Lobb's experiment

The predicted temperatures distribution along the stagnation line of T and $T_{v_{N_2}}$ for five chemical models are shown in Fig.3. The computations are done with Park curve fit equilibrium constants in conjunction with Park CVD coupling. The maximum value of T

and $T_{v_{N_2}}$ behind the shock wave is obtained with the slow kinetic models. It is clearly seen that the vibrational relaxation time for molecular nitrogen in the post shock region is greatest with the slow kinetic models and lowest with the fast kinetic models, caused by higher density in the shock layer which enhances the collisional energy transfer mechanisms. It is observed that all temperatures tend towards a thermodynamic equilibrium near the stagnation point. Note that the features of the flow physics is evident by the existence of a significant thermal nonequilibrium behind the shock wave and, the vibrational temperature remains below the associated translational temperature whatever the choice of chemical kinetic model. The original Dunn and Kang model predicts the lowest temperatures which become as high as the Gardiner prediction when the backward rates are calculated with the Park equilibrium constant.

The predicted pressure distributions along the stagnation line are plotted in Fig.4. It is noted that all chemical models converge to the same peak value of pressure at the stagnation point, and that the difference between the Hansen and Park CVD coupling cannot be discriminated. These distributions are used to identify the shock location. One can see that the shock standoff distance tends to increase when the kinetic velocity is decreased, approaching the frozen flow. The shock standoff distance is the smallest for the case of fast kinetic models, suggesting the higher degree of dissociation compared to other kinetics. The peak temperature, however, is highest for Gardiner model and lowest for Dunn and Kang model, as expected. A comparison with the location given by Lobb[30] is reported in Table 3. The values reported for the shock standoff distance correspond to the point of the maximum pressure gradient associated with the thickness of the mesh. With respect to the shock standoff distance observed in the Lobb experiment (0.087 R_s with a $\pm 5.75\%$ experimental uncertainty), the calculated standoff value predicted using Park's (93) data is 4.36% smaller, while, the value predicted with the Gardiner data is 7.46% greater. The result produced by the Park(93) model is closest to the experimental value.

The evolutions of the calculated wall heat flux are distinct and presented in Fig.5 as a function of the angle θ is affected. The fast kinetic models produce similar profiles. The same observation is made with the slow kinetic models. At the stagnation point, the current chemical models produce stagnation heating values that range from 23 to 38 MW/m^2 . The calculation of the backward reactions with the analytic equilibrium constant tends to increase the wall heat flux with Park's (93) model while Gardiner's model tends to decrease it about 13 MW/m^2 at the stagnation point. The numerical results obtained by other authors are about 25 MW/m^2 [33; 34]. This case demonstrates that Park(93) model with Park curve fit constant has a better prediction of shock stand-off distance and wall heat flux value.

5.1.2 Rose and Stankevics's experiment

Calculations for the second case focus on the Mach 18 air experimental case of Rose. Computed temperature distributions obtained with the Park(93) model along the stagnation line are shown in Fig.6. The backward reaction rates are evaluated either with analytic or Park and/or Gupta equilibrium constants. In the Park(93) model, the manner in which the backward reaction rates are calculated do not affect profiles. The nonequilibrium behavior of the vibrational energy mode can be seen from the temperature profiles near the shock region. It can be seen from the variation of the vibrational temperatures in the vicinity of the shock wave that the vibrational relaxation time for O_2 is the lowest. This figure clearly shows that the influences of the CVD coupling of Park and Hansen are not visible in the Park(93) model. The

evolution of temperatures obtained with the Gardiner model presented in Fig.7 are affected by the method of computation of the backward reactions. Note that the same observation applies to the Mach 15.3 case where the temperatures obtained with the slow kinetic models behind the shock wave are high.

It is important to determine the correct dissociation rate in hypersonic flow, because the degree of dissociation significantly affects the heat transfer, when the surface is catalytic with recombination of atoms (as is the case for most thermal protection materials). Figure 8 shows the heat transfer Q_w along the body surface for four chemical kinetic models. As expected, the higher values of Q_w are obtained with slower kinetics. The stagnation point heat transfer are reported in Table 4 and compared with experimental data[31]. Computed stagnation heat flux is over predicted with Gardiner, Moss and modified Dunn and Kang models. In the attempt to improve Dun and Kang model, a modified Dunn and Kang was obtained with the using of equilibrium constants in the calculation of the backward reactions. The model of Park (93) gives better agreement with the experimental measurement.

When weakly ionization and electron-electronic energy are taken into account in conjunction with chemical model of Park(93), the predicted temperature distribution along the stagnation line is shown in Fig.9. The electronic relaxation and the effects of the modified speed of sound are examined here. The electron-electronic temperature is lower with the correction. This translates that the distribution of the total energy on various internal modes has been a more accurately accounted form in results. The flux splitting procedure and the physics of the flow take into account this correction which allows to approach correctly the local speed of sound in the presence of the electron translational temperature.

5.1.3 RAM-CII experiment

There are no experimental measurements of heat flux in this case, the interest of this study is to submit the chemical models to very high temperatures and to compare numerical results. The graphs presented here are obtained with the Gupta equilibrium constant whose field of validity is wider.

In Fig.10 the translational temperature is around 20 000K and the extrapolation of certain formulations becomes erroneous. For example at this temperature, it is necessary to account for ionization although the chemistry of Moss and Gardiner are conceived only for neutral air gas. There is a significant decrease in the temperature predicted by the modified Dunn and Kang model. These differences indicate that the Dunn and Kang rate set is not consistent with Gupta's equilibrium constants at the higher temperatures associated with Mach 25.9. This conclusion is easily verified for each reaction with a direct comparison of the equilibrium constants to the ratio of rates. Inconsistency with Gupta's equilibrium constants does not assure that, Dunn and Kang rates will not produce correct species distributions. This inconsistency, however, raises doubt as to recommending this rate set as the correct data for these flows.

The surface heat transfer Q_w is shown in Fig.11 for four chemical kinetics models. The difference of peak between calculations with Park CVD coupling and Hansen at the stagnation point is about 2,5%. The maximum value of the heat flux is located at the position $\theta = 0^\circ$. The computed stagnation point heat flux results are compared with other numerical results in Table 5. The large dispersion of the results obtained puts into doubt the accuracy of certain reactions rates, or indicates that some other unknown thermo-chemical process occurs in these flows. The numerical results reported in Table 5 are obtained with a non-catalytic wall. The

numerical methods and the selected chemical model are different. Walpot[36] and Soubrie et al.[37] have used a model with 11-species while a model with 7-species has been considered by others [14; 38]. The flux value for Candler and MacCormack given in Table 5 is estimated from the Stanton number. It is noted that the values obtained with the slow kinetic models are higher. This was encountered in all the cases that were studied.

An extension is made to the case $M_\infty = 23.9$ with a four temperature model and weakly ionized gas considered under Park(93) chemical kinetic. Figure 12 shows the predicted temperature distribution obtained along the stagnation line at Mach 23.9. The comparative evolution of the various temperatures justifies the choice of the model at four temperatures. The difference between $T_{v_{O_2}}$ and $T_{v_{N_2}}$ becomes larger for a strong Mach number in a flow at relatively low density condition. The use of a model at one temperature of vibration can induce miscalculations in the kinetic of the reactions, which will influence the calculation of the thermodynamic parameters. Figure 13 shows the comparison of the computed and the measured peak electron number density along the body for Mach 23.9 and 25.9. The comparison shows very good agreement, with a scatter from the experimental values. Most of the ionization occurs at stagnation region. The electron number density is maximal in the stagnation point of the obstacle and decreases along the body.

5.1.4 Hornung's experiment

Calculations involving hypervelocity nitrogen flow over cylinders are performed under conditions reported in table 2. The results obtained demonstrate the sensitivity of flowfield to the effect of finite rate chemistry. The free-stream gas is composed by nitrogen dissociated partially ($Y_{N_2} = 0.927$, $Y_N = 0.073$). The wall is assumed to be adiabatic and non-catalytic. This case implements the experiment performed by Hornung[32] for 1 inch diameter cylinders with the dissociation of nitrogen at 5.59 km/s. The calculations use three different sets of dissociation rates of N_2 .

The calculations using the corresponding free-stream conditions have been made for the body and figures 14- 16 show interferograms and computed fringe patterns derived from the simulation results. The exact position of the shock in both the experiments and the simulations is uncertain : in the experiments because of the shock curvature in the transverse direction and in the simulations because the shock is smeared over a few cell widths. To compare the experiments and the simulations more closely it is necessary to compare fringe shifts at different locations in the flow. Figure 14 compares the computed interferograms obtained with Dunn and Kang and the Modified Dunn and Kang. In the modified model, the backward rates are calculated with the Gupta curve fit equilibrium constant. The two solutions are quite different. The distance from the detachment of the shock is sensitive to the chemical model selected. Although the Dunn and Kang model is very poor, the modified version improves the thickness of the shock layer.

The fringes for the case with Park(93) and Gardiner with analytic equilibrium constant are plotted in Figs. 15 and 16. The frames are quantitatively well predicted. The experimental and computational interferograms have the same general features, but differ little in the details. The best comparison is obtained with the Park (93) model.

5.2 Interaction of type IVr around a double-wedge in hypersonic flow

Shock/shock interactions are common in many aerodynamic configurations such as those encountered during hypersonic flight, around launchers or in propulsion systems. Such shock

	α	β
N_2	0.90	0.30
O_2	0.85	0.25
NO	0.80	0.30

Table 1. CVD coefficients for Hassen’s model

Experiments	Lobb[30]	Rose[31]	Ram C[13]	RamC[13]	Hornung[32]	Double-Wedge
Gas	Air	Air	Air	Air	N_2, N	Air
$R_s, (mm)$	6.35	6.6	152.4	152.4	0.5 inch	500
M_∞	15.3	18	25.9	23.9	6.14	9
$U_\infty, (m/s)$	5263	5742.49	7658.6	7636.4	5590	3130.137
$P_\infty, (Pa)$	664	432.2	4.764	19.85	2910	10^5
$T_\infty, (K)$	293.0	252	216	254	1833	300
$T_{wall}, (K)$	1000	555.5	1500	1500	adiabatic	adiabatic
Re_∞	14605	12840	6280	19,500	6000	10^5
IM nodes	50	60	70	60	50	400
JM nodes	50	60	70	70	50	500
$\Delta x_{min} (m)$	4.1936×10^{-6}	1.423×10^{-6}	2.002×10^{-5}	2.1171×10^{-5}	4.214×10^{-5}	$4,1122 \times 10^{-6}$
$\Delta y_{min} (m)$	7.2055×10^{-5}	4.6432×10^{-5}	1.27×10^{-4}	2.7318×10^{-4}	1.072×10^{-4}	$2,520 \times 10^{-6}$

Table 2. Detail of free-stream conditions and grids used

interactions can cause high localized heat transfer rates as well as local oscillations of the pressure fields on the vehicle surface. These can alter the aerodynamic characteristics of the vehicle leading to catastrophic failures.

The geometrical constraints and flow field parameters are chosen such as flow generates an interaction of type IVr. After study grid independence, the number of grid points used here is 400×500 . The initial conditions are: $L_1, L_2 = 0.05$ (m); $\theta_1 = 15$; $\theta_2 = 60$; $P_\infty = 10^5 (Pa)$; $T_\infty, T_{V_{N_2}}, T_{V_{O_2}} = 300$ (K);

$U_\infty = 3130.137$ (m/s); $M_\infty = 9.0$; $Re_\infty = 2.0016 \times 10^5 / m$, $Y_{N_2} = 0.766$; $Y_{O_2} = 0.233$.

In this study, a value of $\gamma = 1.4$ is used to initialize calculation because the free-stream flow is assumed as a perfect gas frozen.

The choice of the chemical model (in equilibrium or in nonequilibrium) for use in the numerical simulations of flow around double-wedge can lead to different results. Although widely validated for flow around blunt bodies [15], very large uncertainties remain for the double-wedge. Figure 17 reflects the subtle differences that can be achieved between two kinetics (slow or fast) at thermal equilibrium. Gardiner and Park(93) chemical kinetics are used. A remark that emerges from the different results obtained with the models of Park and Gardiner show that the dissociation rates at the equilibrium appear not to be well known for a flow around a double-wedge.

With Park Consts.	δ/R (%)
Park (93)	8.321
Gardiner	9.349
Moss	9.35
Modified Dunn and Kang	9.930
Dunn and Kang	7.650
Lobb - Experiment[30]	8.7±0.5

Table 3. Shock stand-off distance, $M_\infty = 15.3$

Chemical kinetics with K_{eq} :	Park	Gupta
Park (93)	44.95	45.5
Gardiner	47.0	47.4
Moss	48.5	49.2
Modified Dunn and Kang	49.0	50.1
Dunn and Kang		32.5
Fay-Ridell[35]		45.0
Experiment- Rose et al.[31]		46.0

Table 4. Stagnation heat flux Q_w (MW/m^2), with Park CVD coupling, Mach 18

Source	Chemical model	Q_w (MW/m^2)
Present	D & K	0.58
Present	Park (93)	1.02
Present	Gardiner	1.91
Present	D & K + Gupta	2.42
Present	Moss	2.63
Walpot[36]	Park(93)	0.74
Walpot[36]	D & K	0.90
Soubrié et al.[37]	Park(93)	0.96
Candler et al.[38]	Park & Wray	2.5

Table 5. Stagnation heat flux, RAM-CII, Mach 25.9

IntechOpen

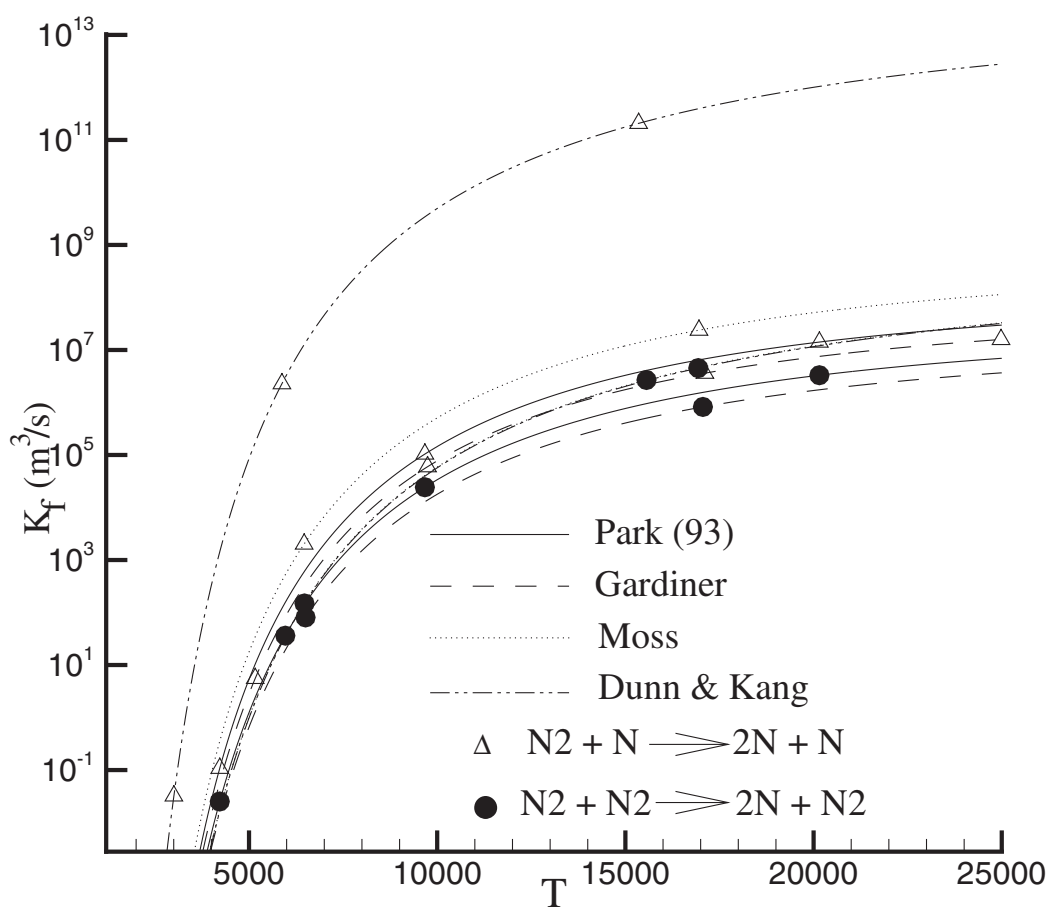


Fig. 1. Forward reactions rate

IntechOpen

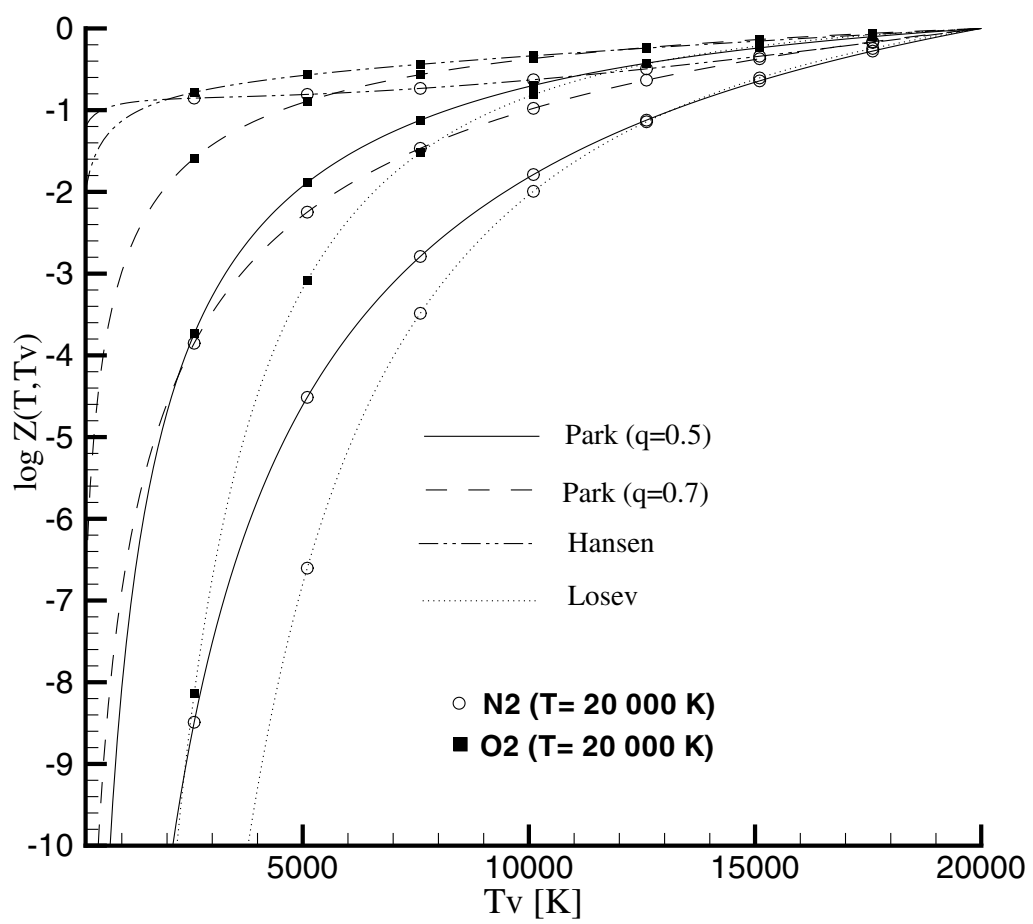


Fig. 2. Coupling factor $Z(T, T_v)$ for O_2 and N_2

IntechOpen

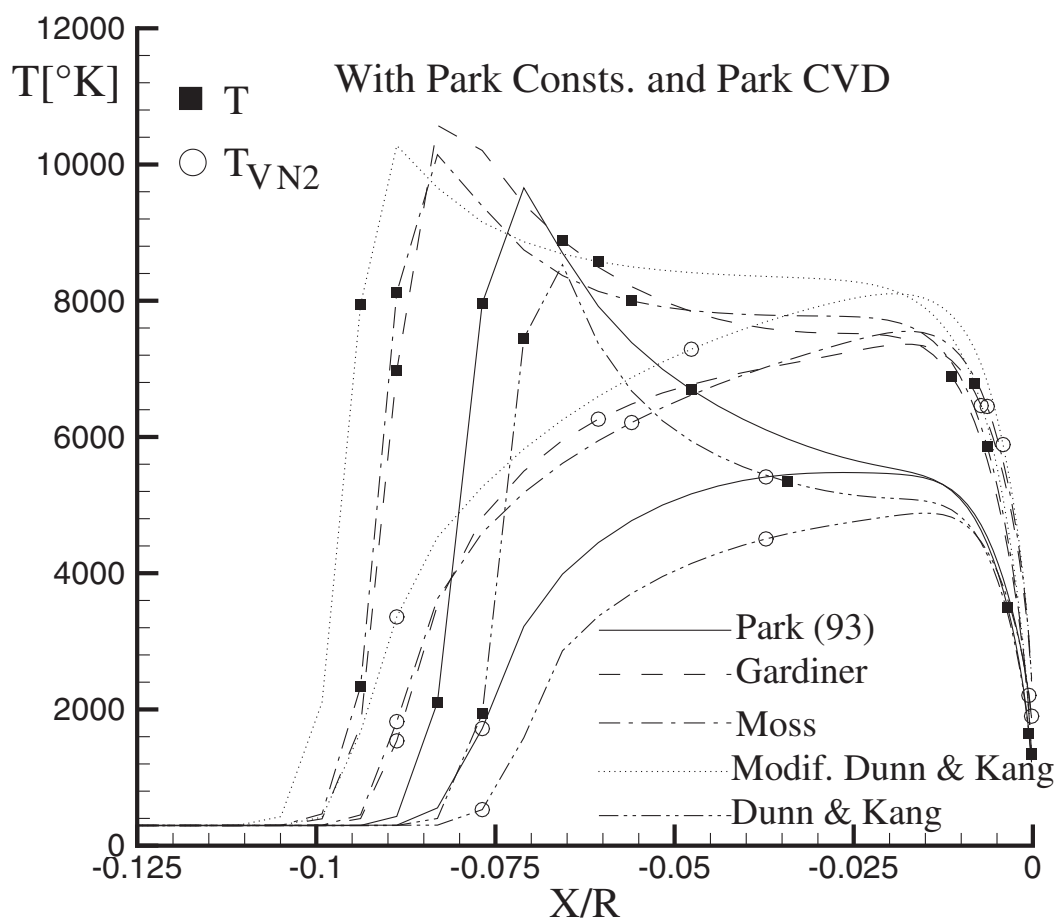


Fig. 3. Temperatures along the stagnation line, $M_\infty=15.3$

IntechOpen

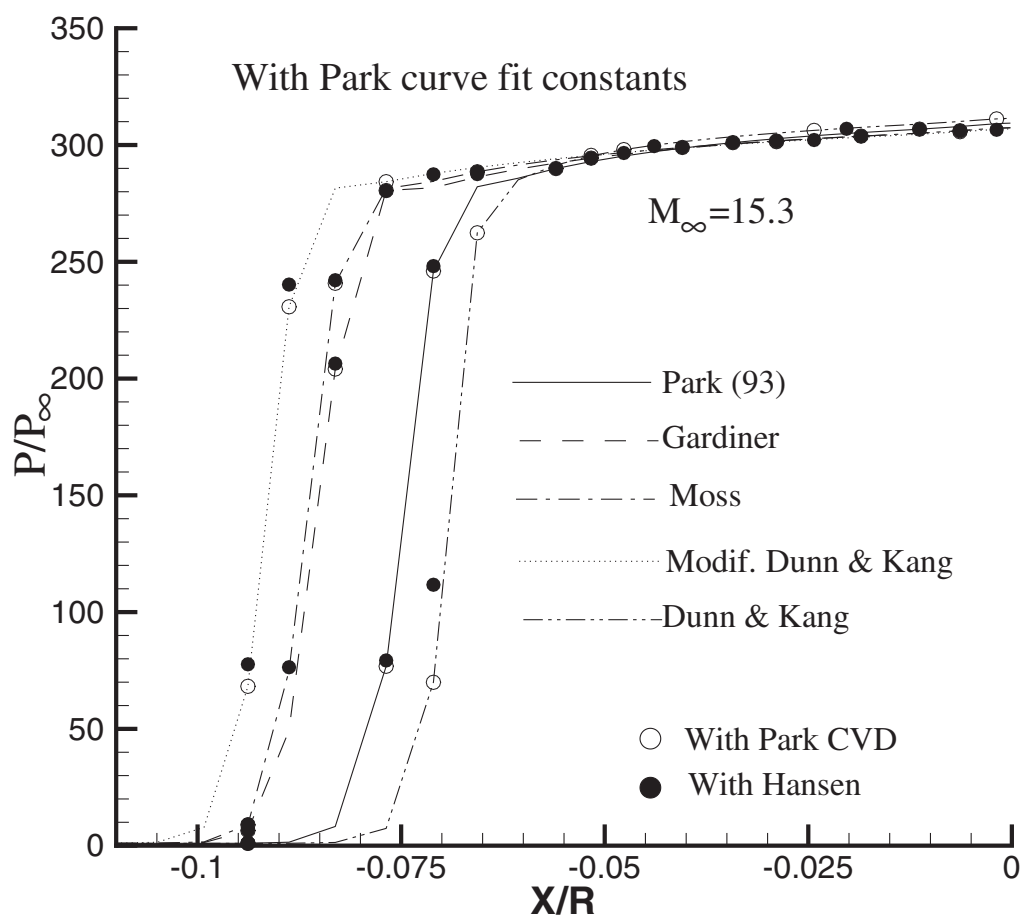


Fig. 4. Pressure distribution along the stagnation line, $M_\infty = 15.3$

IntechOpen

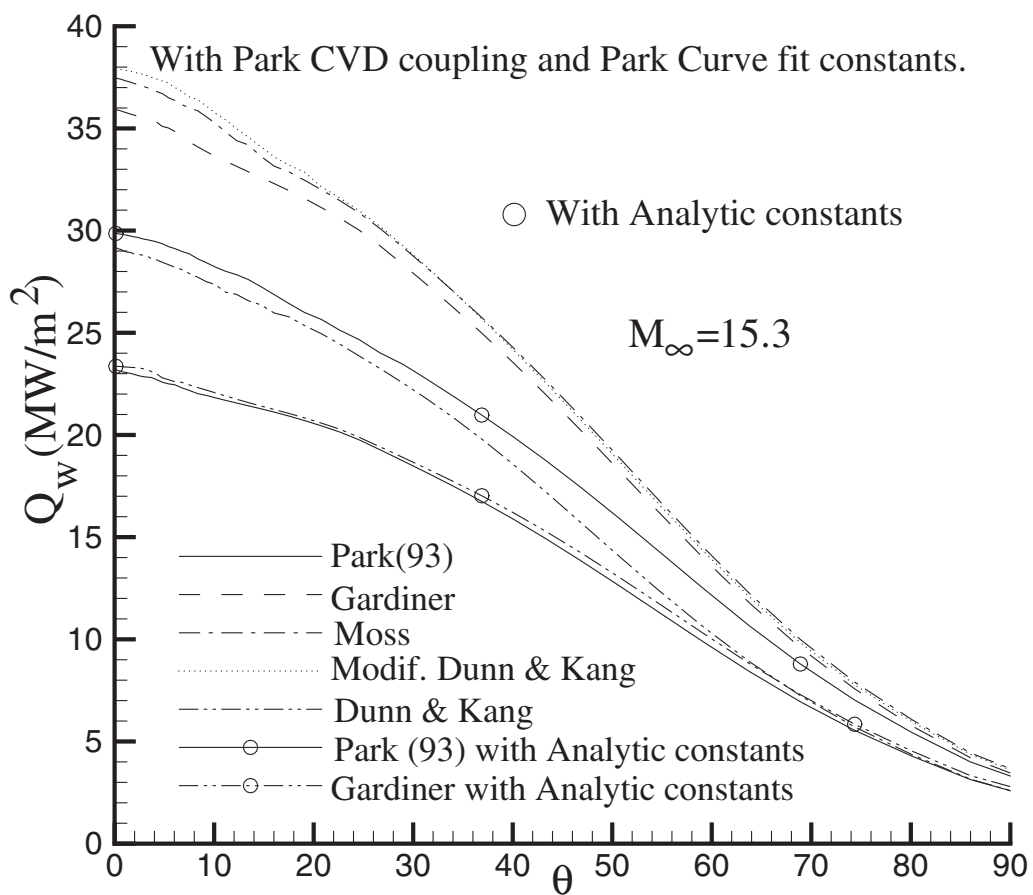


Fig. 5. Wall heat flux, $M_\infty=15.3$

IntechOpen

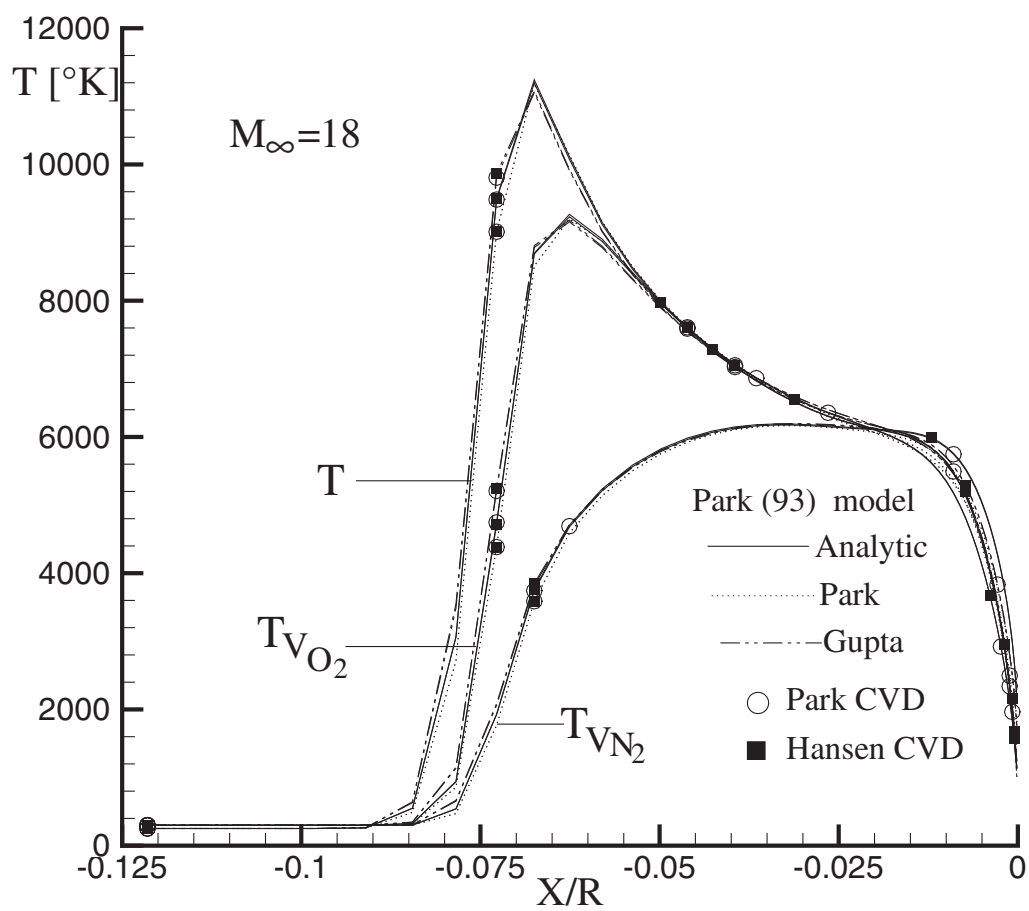


Fig. 6. Temperatures with Park(93) model, $M_\infty=18$

IntechOpen

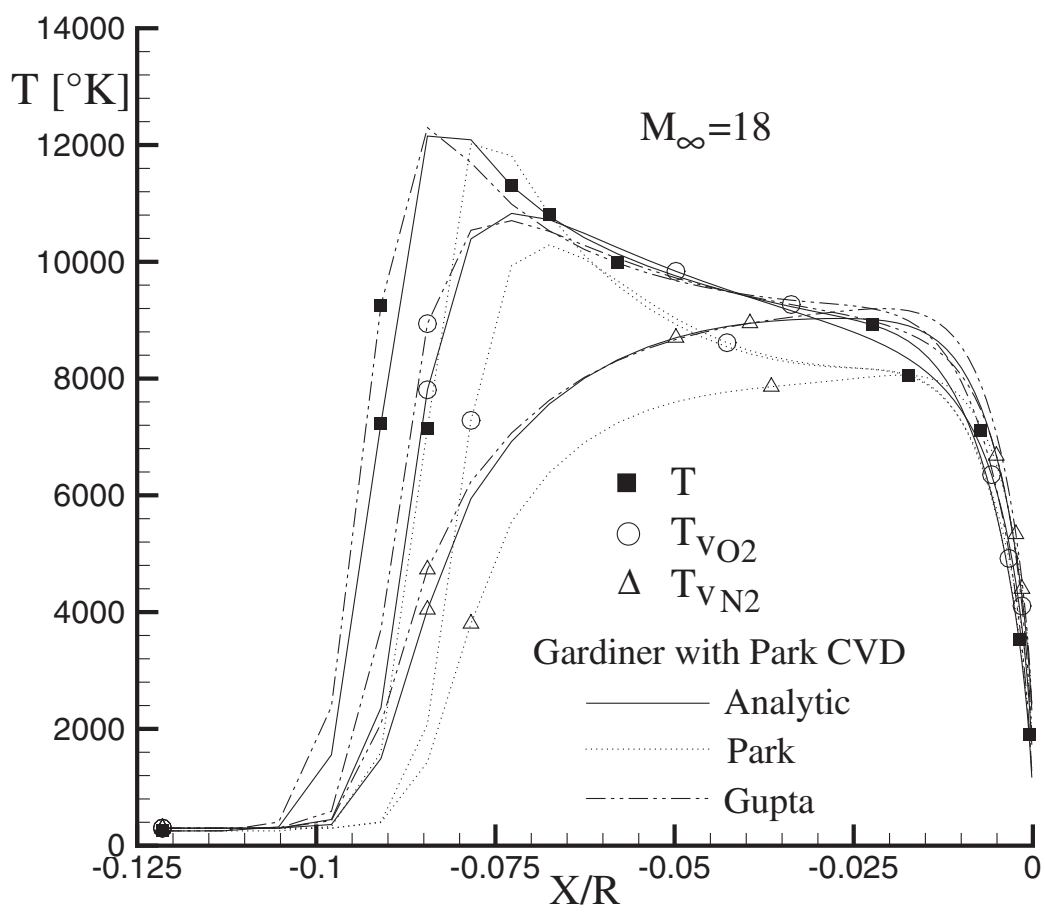
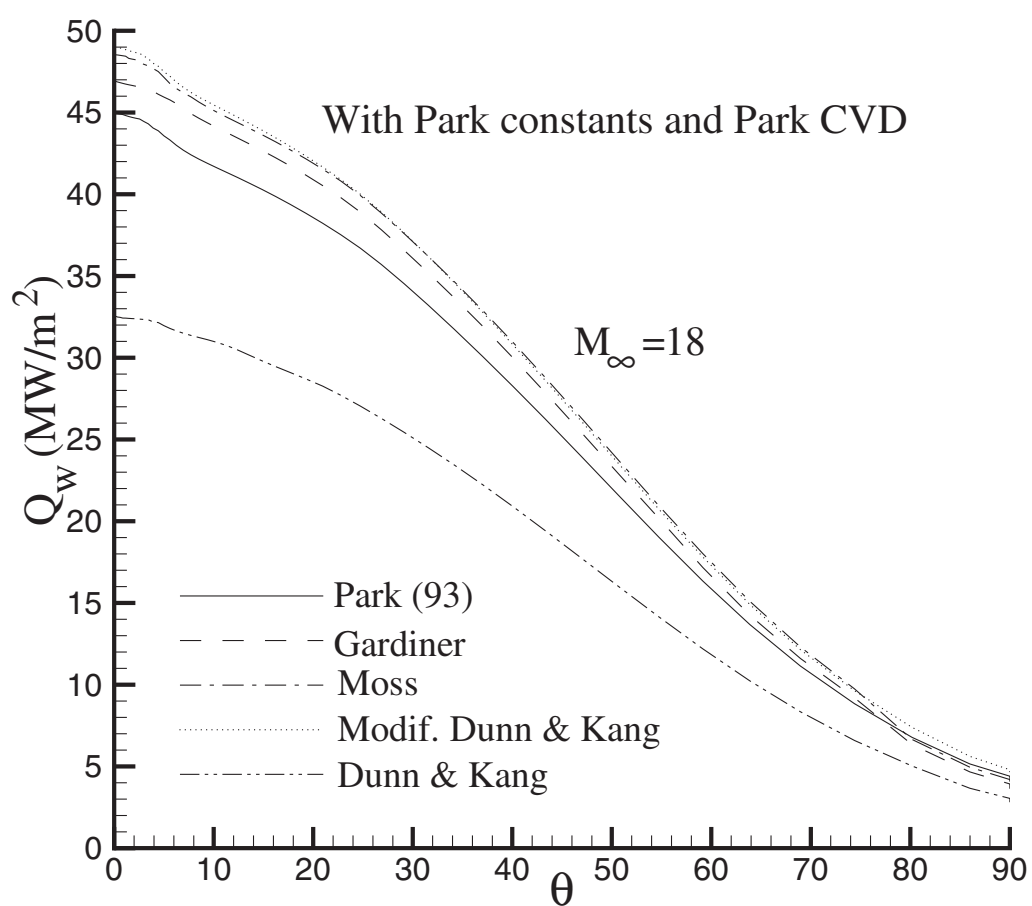


Fig. 7. Temperatures profile with Gardiner model, $M_\infty=18$

IntechOpen

Fig. 8. Wall heat flux, $M_\infty=18$

Introduction

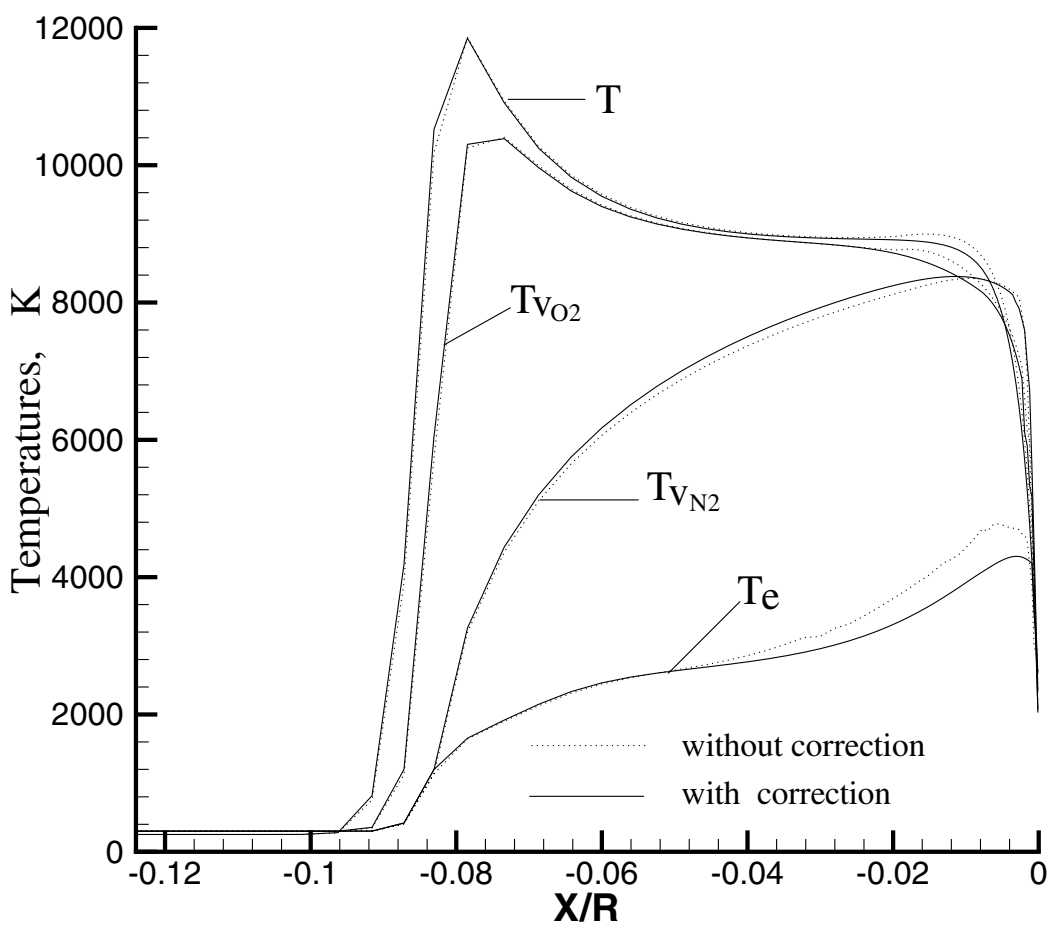


Fig. 9. Temperature along stagnation line with weakly ionized gas; $M_\infty = 18$

IntechOpen

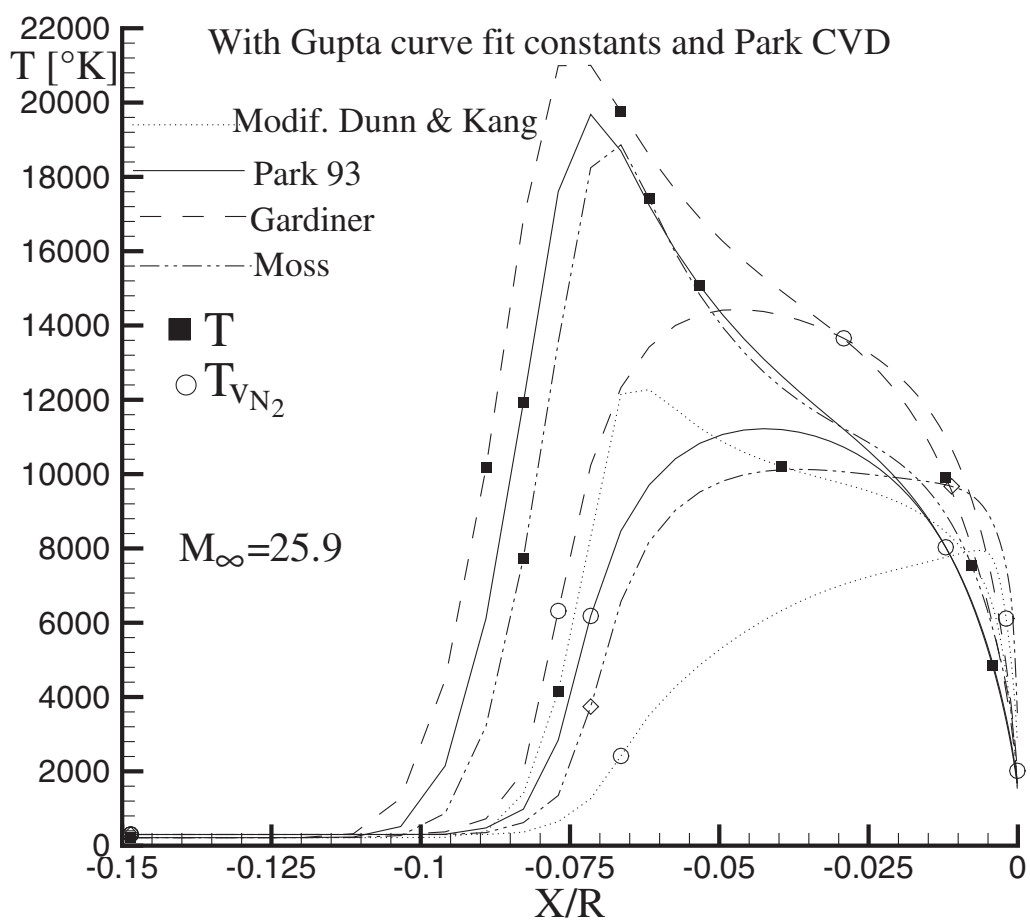


Fig. 10. Temperature profile with Gupta curve fit constants, $M_\infty=25.9$

IntechOpen

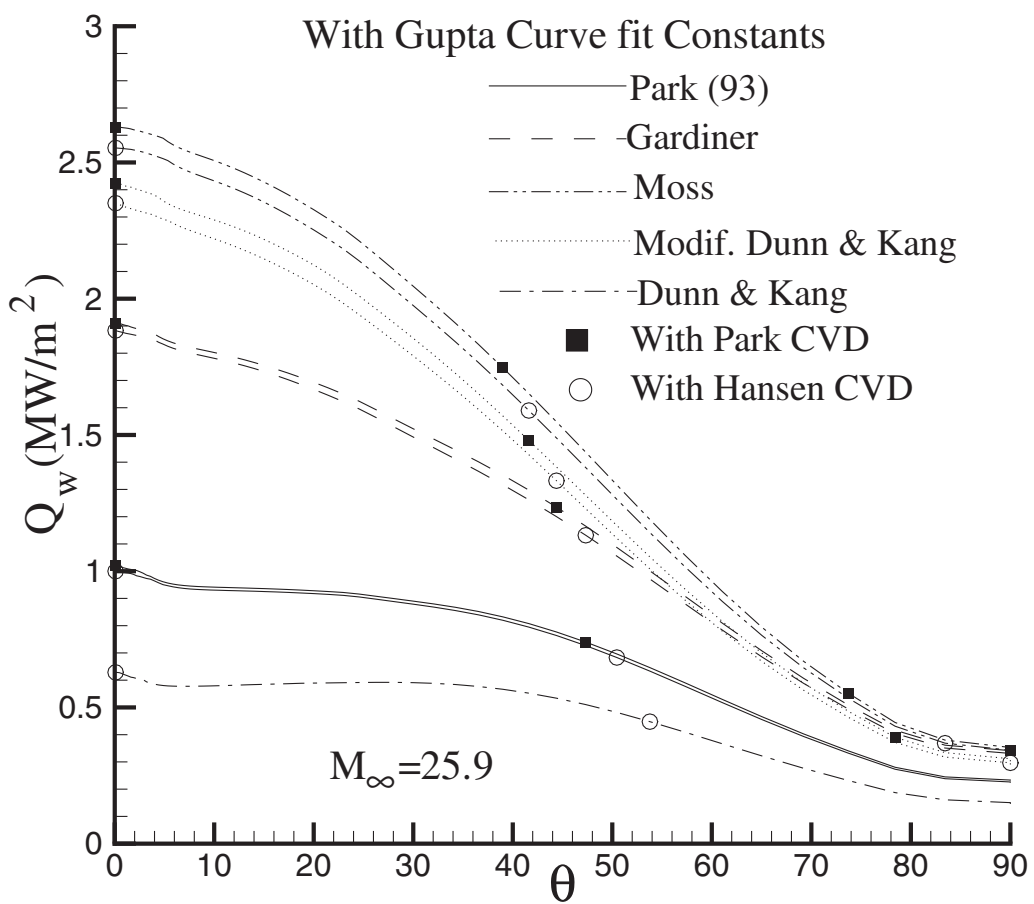


Fig. 11. Stagnation heat flux, $M_\infty=25.9$

IntechOpen

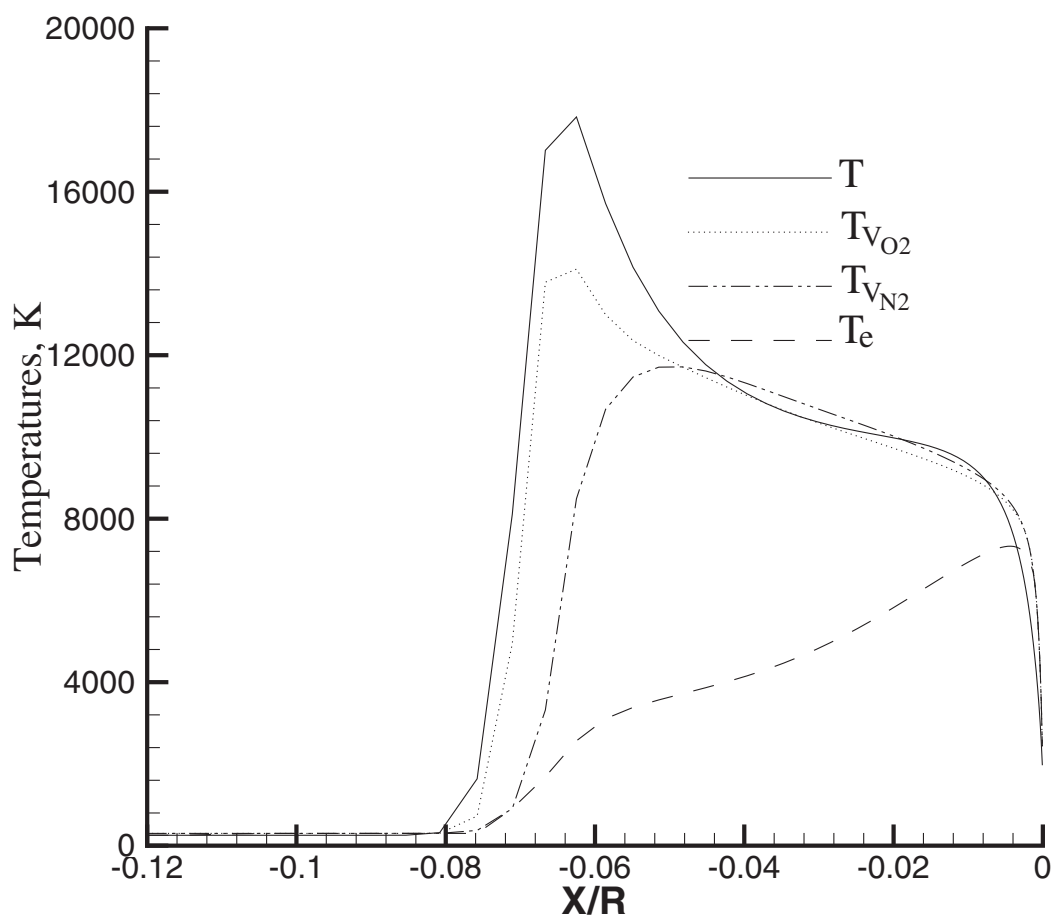


Fig. 12. Temperatures distribution along the stagnation line, $M_\infty=23.9$

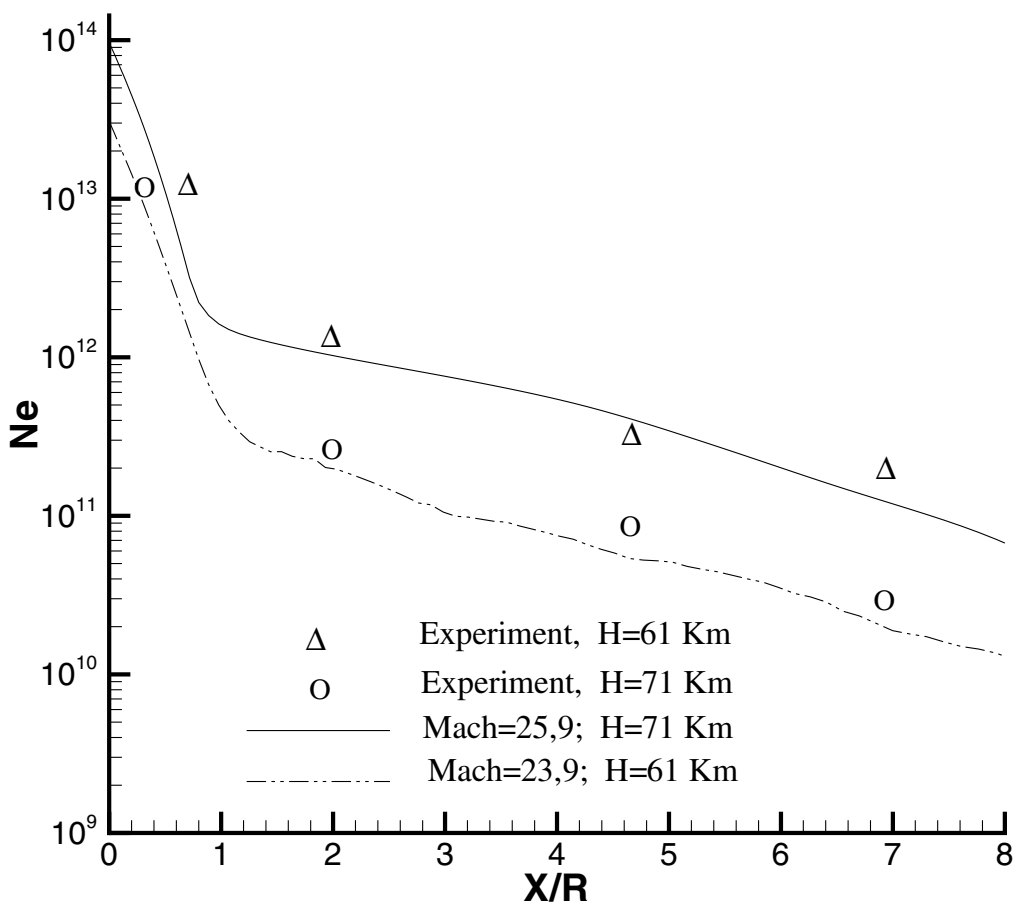


Fig. 13. Comparison with experiment of the peak of electron number density following the axial distance

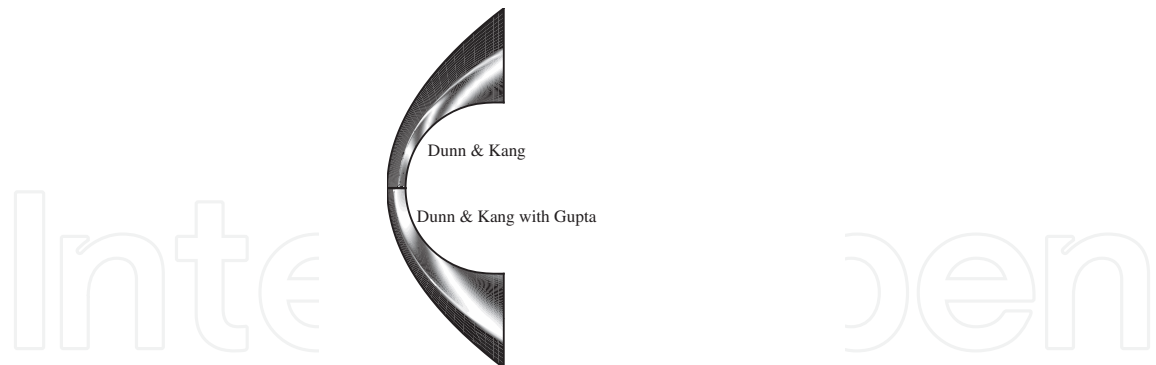


Fig. 14. Dunn and Kang, and Modified Dunn and Kang Interferograms computed

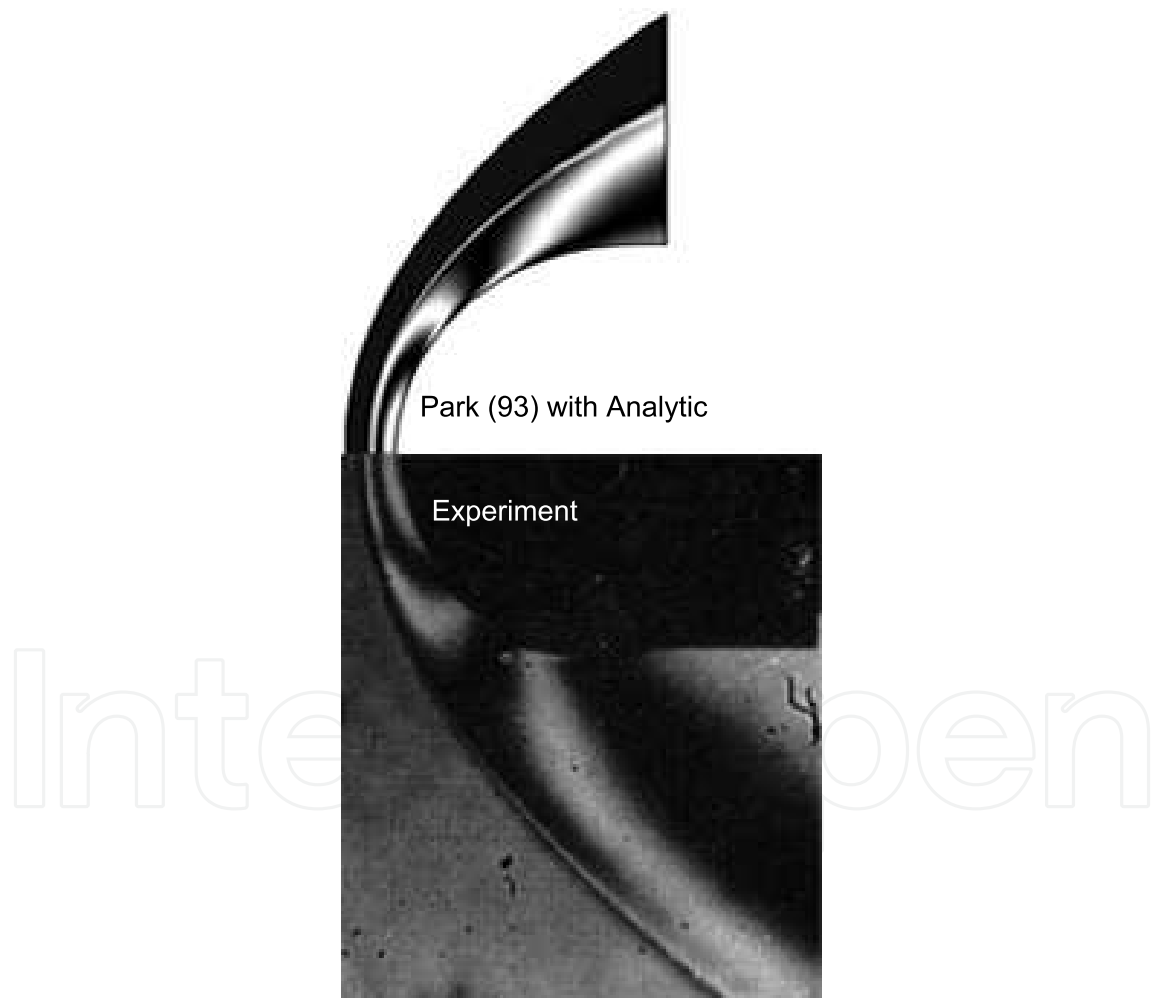


Fig. 15. Fringe patterns on 1 in diameter cylinder with Park(93) model and Exact equilibrium constant

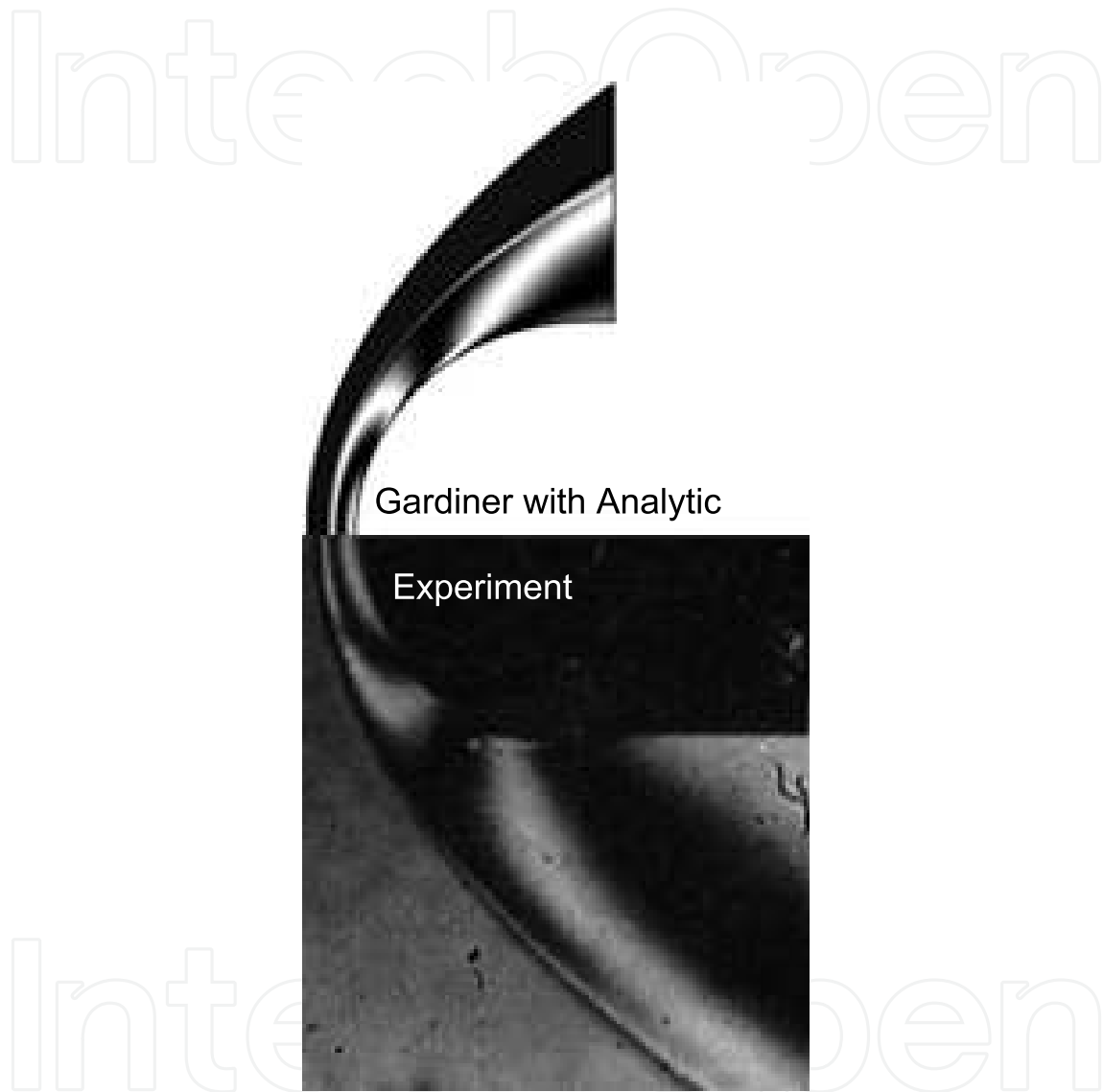


Fig. 16. Fringe patterns on 1 in diameter cylinder with Gardiner model and Exact equilibrium constant

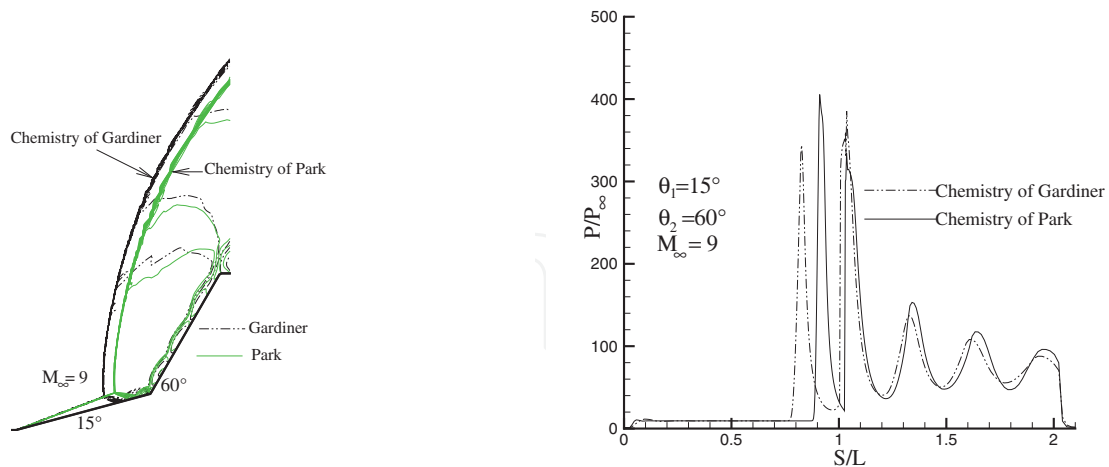


Fig. 17. Effect of chemical kinetics: a) Contours Mach number b) Surface pressure

6. Conclusion

The hypersonic flow past blunt bodies with thermo-chemical nonequilibrium were numerically simulated. The dependence of solutions on available chemical models, allowing to assess the accuracy of finite rate chemical processes has been examined. The present results were successfully validated with the theoretical and experimental work for shock-standoff distances, stagnation point heat transfer and interferograms of the flow. Although all model describe the essential aspects of the nonequilibrium zone behind the shock, they are not accurate for the evaluation of the aerothermodynamic parameters. A comparative study of various kinetic air models is carried out to identify the reliable models for applications with a wide range of Mach number.

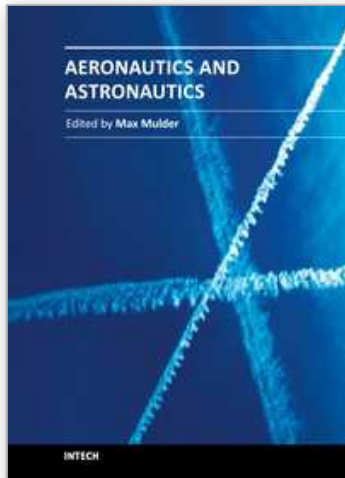
The present study has shown that the prediction of hypersonic flowfield structures, shock shapes, and vehicle surface properties are very sensitive to the choice of the kinetic model. The large dispersion in the wall heat flux reaches 60 % as observed in the RAM-CII case. The manner in which the backward reaction rates are computed is quite important as indicated by the interferograms that were obtained. The model of Park (93) gives a better prediction of hypersonic flowfield around blunt bodies. Park(93) is identify as the model for hypersonic flow around blunt bodies with a confidence acceptable to a wide range of Mach number. There is also great sensitivity to the choice of chemical kinetics in flowfield around double-wedge. More numerical simulations compared with experiments need to be conducted to improve the knowledge of the thermochemical model of air flow around double-wedge.

7. References

- [1] Park, C. (1990). *Nonequilibrium Hypersonic Aerothermodynamics*. New York, Wiley.
- [2] Gupta, R. N., Yos, J. M., Thompson, R. A., and Lee, K. P. (1990). A Review of Reaction Rates and Thermodynamic and Transport Properties for an 11-Species Air Model for Chemical and Thermal Nonequilibrium Calculations to 30 000K", *NASA RP-1232*.
- [3] Vincenti, W. G., Jr. Kruger, C. H. (1965). *Introduction to physical Gas Dynamics*. Krieger, FL.
- [4] Gardiner, W. C. (1984). *Combustion Chemistry*, Springer-Verlag, Berlin.

- [5] Shinn, J. L., Moss, J. N., Simmonds, A. L. (1982). Viscous Shock Layer Heating Analysis for the Shuttle Winward Plane Finite Recombination Rates, AIAA 82-0842.
- [6] Dunn, M. G., Kang, S. W. (1973). Theoretical and Experimental Studies of re-entry Plasma, NASA CR-2232.
- [7] Park, C. (1993). Review of Chemical-Kinetic Problems of Future NASA Mission, I: Earth Entries", *Journal of Thermophysics and Heat Transfer*. Vol. 7, No. 3, pp. 385-398.
- [8] Hansen, C. F. (1993). Vibrational Nonequilibrium Effect on Diatomic Dissociation Rates". *AIAA Journal*, Vol. 31, No. 11, pp. 2047-2051.
- [9] Macrossan, N. M. (1990). Hypervelocity flow of dissociating nitrogen downstream of a blunt nose. *Journal of Fluid Mechanics*, Vol. 27, pp. 167-202.
- [10] Josyula, E. (2001). Oxygen atoms effect on vibrational relaxation of nitrogen in blunt body flows. *Journal of Thermophysics and Heat Transfer*, Vol. 15, No. 1, pp. 106-115.
- [11] Peter, A. G. and Roop, N. G. and Judy, L. S. (1989). Conservation Equation and Physical Models for Hypersonic Air flows in Thermal and Chemical Nonequilibrium. NASA TP 2867.
- [12] Knab, O. and Fruaudf, HH. and Messerschmid, EW. (1995). Theory and validation of the the physically consistent coupled vibration-chemistry-vibration model. *J. Thermophys Heat Transfer*, nř9, Vol.2, pp.219-226.
- [13] Tchien G., Burtschell Y., and Zeitoun E. D. (2008). Computation of non-equilibrium hypersonic flow with Artificially Upstream Flux vector Splitting (AUFS) schemes. *International Journal of Computational Fluid Dynamics*, Vol. 22, Nř4, pp. 209 - 220.
- [14] Tchien G., and Zeitoun D. E. (2008). Computation of thermo-chemical nonequilibrium weakly ionized air flow over sphere cones. *International journal of heat and fluid flow*, Vol.29, Issue 5, pp.1393 - 1401.
- [15] Tchien G., and Zeitoun D. E. (2009). Effects of chemistry in nonequilibrium hypersonic flow around blunt bodies. *Journal of Thermophysics and Heat Transfer*, Vol. 23, Nř 3, pp.433-442.
- [16] Burtschell Y., Tchien G., and Zeitoun E. D. (2010). H₂ injection and combustion in a Mach 5 air inlet through a Viscous Mach Interaction. *European Journal of Mechanics B/fluid*, Vol. 29, Issue 5, pp. 351-356.
- [17] Lee Jong-Hun. (1985). Basic Governing Equations for the Flight Regimes of Aeroassisted Orbital Transfer Vehicles. *Thermal Design of Aeroassisted Orbital Transfer Vehicles*, H. F. Nelson, ed., Volume 96 of progress in Astronautics and Aeronautics, American Inst. of Aeronautics and Astronautics, Vol. 96, pp. 3-53.
- [18] Appleton, J. P. and Bray, K. N. C. (1964). The Conservation Equations for a Nonequilibrium Plasma. *J. Fluid Mech.* Vol. 20, No. 4, pp. 659-672.
- [19] Tchien, G., Burtschell, Y., and Zeitoun, E. D., 2005. Numerical study of nonequilibrium weakly ionized air flow past blunt body. *Int. J. of Numerical Methods for heat and fluid flow*, 15 (6), 588 - 610.
- [20] Blottner, F. G., Johnson, M., and Ellis, M., 1971. Chemically Reacting Viscous Flow Program for Multi-Component Gas Mixtures. Sandia Laboratories, Albuquerque, NM, Rept. Sc-RR-70-754.
- [21] Wilke, C. R., 1950. A viscosity Equation for Gas Mixture. *J. of Chem. Phys.* 18 (4), 517-519.
- [22] Ramsaw JD., and Chang CH., 1993. Ambipolar diffusion in two temperature multicomponent plasma. *Plasma Chem Plasma process.* 13 (3), 489-498.

- [23] Masson, E. A., and Monchick, 1962. Heat Conductivity of Polyatomic and Polar Gases. *The Journal of Chemical*. 36 (6), 1622-1640.
- [24] Ahtye, W. F., 1972. Thermal Conductivity in Vibrationally Excited Gases. *Journal of Chemical Physics*, 57, 5542-5555.
- [25] Candler, G. V., and MacCormack, R. W., 1991. Computation of weakly ionized hypersonic flows in thermochemical nonequilibrium. *Journal of Thermophysics and heat transfer*, 5 (3), 266-273.
- [26] Taylor R., Camac, M., and Feinberg, M., 1967. Measurement of vibration-vibration coupling in gas mixtures, In *Proceeding of the 11th International Symposium on combustion*, Pittsburgh, PA, 49-65.
- [27] Sharma, S. P., Huo, W. M., and Park, C., 1988. The Rate Parameters for Coupled Vibration-Dissociation in a Generalized SSH Approximation Flows. AIAA-88-2714.
- [28] Shatalov, O. P., and Losev, S. A., "Modeling of diatomic molecules dissociation under quasistationary conditions", AIAA 97-2579, 1997.
- [29] Roe, P., 1983. Approximate Riemann Solvers, Parameters vectors and difference schemes. *Journal of Computational Physics*, Vol. 43, 357-372.
- [30] Lobb, K., "Experimental measurement of shock detachment distance on sphere fired in air at hypervelocities", in *The High Temperature Aspect of Hypersonic Flow*. ed. Nelson W. C., Pergamon Press, Macmillan Co., New York, 1964.
- [31] Rose, P. H., Stankevics, J. O., "Stagnation-Point Heat Transfer Measurements in Partially Ionized Air". *AIAA Journal*, Vol. 1, No. 12, 1963, pp. 2752-2763.
- [32] Hornung, H. G., "Non-equilibrium dissociating nitrogen flow over spheres and circular cylinders". *Journal of Fluid Mechanics*, Vol. 53, 1972, pp. 149-176.
- [33] Joly, V., Coquel, F., Marmignon, C., Aretz, W., Metz, S., and Wilhelmi, H., "Numerical modelling of heat transfer and relaxation in nonequilibrium air at hypersonic speeds", *La Recherche Aérospatiale*, Vol.3, 1994, pp. 219-234.
- [34] Séror, S., Schall, E., and Zeitoun, E. D., "Comparison between coupled euler/defect boundary-layer and navier-stokes computations for nonequilibrium hypersonic flows, *Computers & Fluids*, Vol.27, 1998, pp. 381-406.
- [35] Fay, J. A., Riddell, F. R., "Theory of stagnation point heat transfer in dissociated air". *J. Aero. Sciences*, Vol. 25, 1958, pp. 73-85.
- [36] Walpot, L. M., "Development and Application of a Hypersonic Flow Solver". PhD thesis, TU Delft, 2002.
- [37] Soubrié, T., Rouzaud, O., Zeitoun, E. D., "Computation of weakly multi-ionized gases for atmospheric entry using an extended Roe scheme". ECCOMAS, Jyväskylä, 2004.
- [38] Candler, V. G., MacCormack, W. R., "The computation of hypersonic ionized flows in chemical and thermal nonequilibrium". AIAA 88-0511, 1988.



Aeronautics and Astronautics

Edited by Prof. Max Mulder

ISBN 978-953-307-473-3

Hard cover, 610 pages

Publisher InTech

Published online 12, September, 2011

Published in print edition September, 2011

In its first centennial, aerospace has matured from a pioneering activity to an indispensable enabler of our daily life activities. In the next twenty to thirty years, aerospace will face a tremendous challenge - the development of flying objects that do not depend on fossil fuels. The twenty-three chapters in this book capture some of the new technologies and methods that are currently being developed to enable sustainable air transport and space flight. It clearly illustrates the multi-disciplinary character of aerospace engineering, and the fact that the challenges of air transportation and space missions continue to call for the most innovative solutions and daring concepts.

How to reference

In order to correctly reference this scholarly work, feel free to copy and paste the following:

Ghislain Tchien and Yves Burtshell (2011). Physico - Chemical Modelling in Nonequilibrium Hypersonic Flow Around Blunt Bodies, *Aeronautics and Astronautics*, Prof. Max Mulder (Ed.), ISBN: 978-953-307-473-3, InTech, Available from: <http://www.intechopen.com/books/aeronautics-and-astronautics/physico-chemical-modelling-in-nonequilibrium-hypersonic-flow-around-blunt-bodies>

INTECH
open science | open minds

InTech Europe

University Campus STeP Ri
Slavka Krautzeka 83/A
51000 Rijeka, Croatia
Phone: +385 (51) 770 447
Fax: +385 (51) 686 166
www.intechopen.com

InTech China

Unit 405, Office Block, Hotel Equatorial Shanghai
No.65, Yan An Road (West), Shanghai, 200040, China
中国上海市延安西路65号上海国际贵都大饭店办公楼405单元
Phone: +86-21-62489820
Fax: +86-21-62489821

© 2011 The Author(s). Licensee IntechOpen. This chapter is distributed under the terms of the [Creative Commons Attribution-NonCommercial-ShareAlike-3.0 License](#), which permits use, distribution and reproduction for non-commercial purposes, provided the original is properly cited and derivative works building on this content are distributed under the same license.

IntechOpen

IntechOpen